International Journal of Fracture 26 (1984) 85–98.

Persistence of the HRR fields for general yielding in mode II

R. BRADFORD

Central Electricity Generating Board, South Western Region, Bedminster Down, Bristol, England

(Received November 30, 1983)

Abstract

The finite element program BERSAFE is used to analyse an edge-cracked square plate under mode II loading in the elastic-plastic regime. Plane strain constraint and power law hardening with $n = 3$ are assumed. Crack tip stress and strain fields are investigated and shown to equal the HRR fields at all loads from small scale yielding through into general yielding.

1. Introduction

In the case of linear elastic fracture mechanics (LEFM), and confining attention to stressing in a single mode, the stresses, σ_{ij}, and strains ϵ_{ij}, sufficiently close to the crack tip can be written in the form,

$$\sigma_{ij}, \epsilon_{ij} = KF_{ij}^{\sigma,\epsilon}(r, \theta) \tag{1}$$

where r, θ are the polar crack tip co-ordinates, and K is the LEFM stress intensity. (Subscripts on K and F denoting the mode have been supressed.) The case for considering a critical value of K to be a material property characterising fracture lies in the fact that the LEFM functions $F_{ij}^{\sigma,\epsilon}$ are independent of body geometry and loading, providing the mode is unchanged. Consequently, two dissimilar bodies subject to the same K will be subject also to identical crack tip fields. In as far as fracture is a response to those crack tip fields, both bodies, composed of the same material, will fracture at the same value of K.

By analogy with the LEFM case, one might initially hope, from a position of ignorance, that in the general elastic-plastic case some functions $g_{ij}^{\sigma,\epsilon}$ might exist such that, sufficiently close to the crack tip, the plastic fields take the form,

$$\sigma_{ij}, \epsilon_{ij} = g_{ij}^{\sigma,\epsilon}(r, \theta, J) \tag{2}$$

where J is some scalar parameter, and where the functions $g_{ij}^{\sigma,\epsilon}$ are universal in the sense that they do not depend upon the body geometry or the loading (beyond the proviso that the mode is unchanged), although they may depend upon material behaviour. The only essential difference between (1) and (2) is that in (2) we have not assumed the crack tip fields to respond linearly to the applied load, and hence have written J (as yet undefined) inside the function g. It is important to realize that the actual functional dependence of the g-functions on r, θ and J is of no consequence. The case for regarding a "critical" (characteristic) value of J to represent the occurrence of fracture/crack growth lies only in the universality of the g-functions.

Unfortunately, in the general case, such universal g-functions either do not exist or do not accurately represent the crack tip fields over a region sufficient in extent to encompass

that in which metallurgical events leading to crack growth (the "process zone") take place. Within the process zone, the g-functions may depend both upon the body geometry and the magnitude of the applied load. However in the special case of small scale yielding, when the plastic zone around the crack tip is small compared to all other relevant dimensions, the g-functions will be universal as long as the load is sufficiently small to maintain the assumption of small scale yielding. This follows because in this case the plastic zone will be surrounded by an elastic region in which the LEFM fields apply, and these fields effectively constitute a boundary condition determining the plastic crack tip fields. The universality of the latter then follows from that of the former. In the case of power law hardening with index n, the universal small-scale yielding plastic fields can be written,

$$\sigma_{ij}, \epsilon_{ij} = G_{ij}^{\sigma,\epsilon}(r/J, \theta, n) \tag{3}$$

and are known as the HRR fields after the original authors, Hutchinson [1], and Rice and Rosengren [2]. In this expression we have taken J to be the path integral of Eshelby [3] and Rice [4].

As the load is increased so that yielding becomes large scale or general, the process zone fields cannot be assumed to retain the form given by (3). (From now on we are assuming power law hardening.) Although this cannot be assumed *in general* it is nevertheless the case that some geometries do retain the crack tip field dependence given by (3) even well into general yielding. Thus, for mode I edge-cracked bend geometries this has been demonstrated using finite element techniques by McMeeking and Parks [5], Shih and German [6] and Needleman and Tvergaard [7]. From these analyses it follows that a characteristic value of $J(J_i)$ determines the initiation of crack growth in bend specimens provided that the size of the uncracked ligament, L, obeys, roughly,

$$L > \frac{25J_i}{\sigma_0} \tag{4}$$

where σ_0 is a suitable "yield" stress. (It is, perhaps, necessary to point out that [5] and [7] use a finite strain formulation in which crack tip geometry changes cause departures from the HRR fields, (3), since the latter have been derived assuming the infinitesimal strain formulation. However, the important point is that the observed fields are universal.)

The same analyses have also shown that for Centre Cracked Panels (CCP) in tension the crack tip fields start to deviate from their small scale yielding forms at relatively lower loads. For this geometry J_i is the characterising property only if the ligament L exceeds, roughly,

$$L > \frac{200J_i}{\sigma_0}. \tag{5}$$

This is sometimes expressed by saying that the CCP geometry, or the associated J_i value, is "valid" when (5) is obeyed.

In this work the crack tip fields are derived, using the finite element program BERSAFE [8,9], for an edge-cracked square plate under mode II (shear) loading. The object of the analysis is to determine whether the crack tip fields in general yielding are equal to the HRR fields, (3). From the foregoing discussion, this is of direct relevance to the feasibility of obtaining valid mode II toughness values for relatively tough, ductile materials, from tests on small specimens. The nature of the loading assumed is rather idealized and probably not easily achievable experimentally, although convenient for academic purposes. However, the present results should form a useful preliminary to the study of more realistic specimen geometries.

2. The finite element model

The elastic-plastic finite element program BERSAFE [8,9] has been used. This program uses an infinitesimal strain formulation, incremental plasticity and isotropic hardening. Stress-strain data are supplied as a discrete set of points, and in uniaxial form. In this work, power law hardening with $n = 3$ is assumed, as follows,

$$\epsilon = \frac{\sigma^3}{E\sigma_0^2} \qquad \text{for} \quad \epsilon > \epsilon_0 \tag{6}$$

where ϵ, σ are the uniaxial (tensile) strain and stress, E is Young's modulus (210×10^3 MPa) and σ_0 is the proportionality-limit stress (taken as 210 MPa). Elastic behaviour is given by $\epsilon = \sigma/E$ for $\epsilon < \epsilon_0$ and hence $\epsilon_0 = \sigma_0/E = 10^{-3}$. In the elastic regime Poisson's ratio, ν, was set to 0.3. The von-Mises (J_2) yield criterion was used, and plane strain constraint was assumed.

Figure 1(a) shows the outer part of the mesh employed. This represents a square plate with an edge crack whose tip lies at the centre of the plate. Loading is accomplished by applying a uniform shearing traction over the face AB, and an equal and opposite shear across face CD. The resulting moment is reacted by fixing the faces BC and DA in the y (but not the x) direction. This fixing includes the nodes on both sides of the crack mouth, but no other crack surface nodes. The midside node of face BC is fixed in the x direction to remove the rigid body degree of freedom. In the absence of the crack, this loading would result in uniform pure shear throughout the whole mesh. In this sense, the loading geometry represents an academic ideal.

The mesh is taken to be of side (W) 100 mm with crack length $a = 50$ mm and of 1 mm thickness. Inside the central crack tip region of Fig. 1(a) fits the refined sub-mesh shown

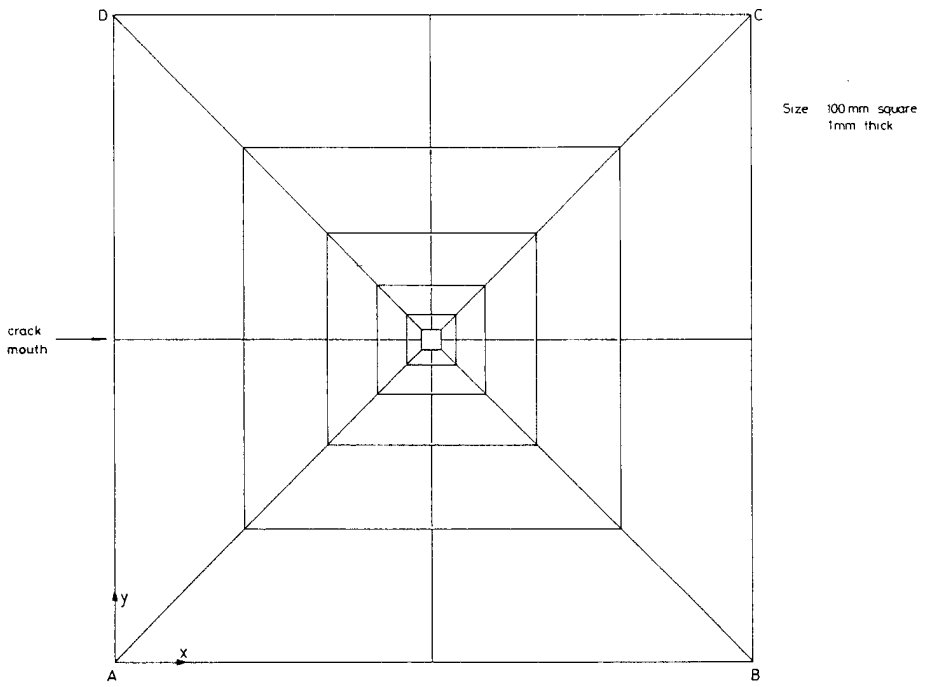

Figure 1(a). Finite element mesh, outer mesh.

in Fig. 1(b), which in turn contains the sub-mesh of Fig. 1(c). The mesh is therefore highly refined in the sense that the ratio of the mesh size to the crack tip element size is very large ($100\ \text{mm} \div 0.5\ \mu\text{m} = 2 \times 10^5$). On the other hand only 96 elements have been used. These are 8 noded, quadrilateral, isoparametric elements with quadratic shape functions.

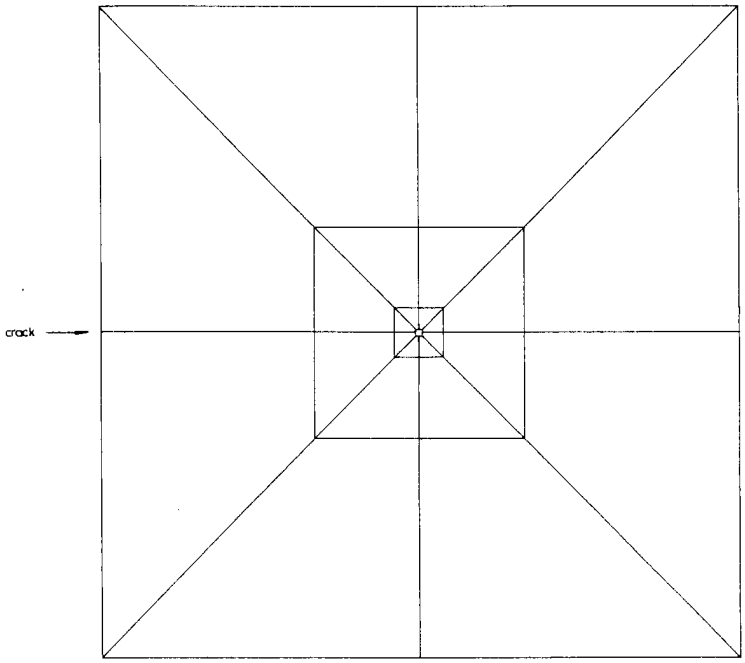

Figure 1(b). Finite element mesh, refined region.

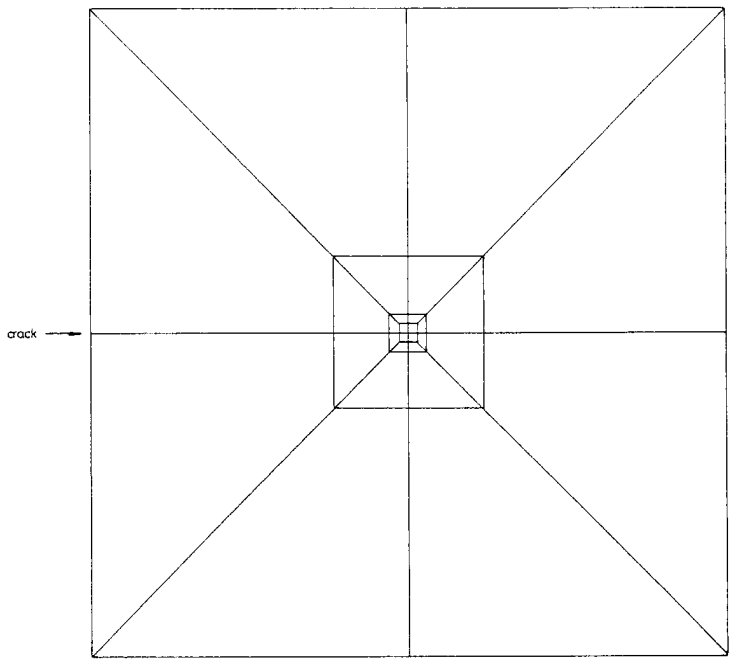

Figure 1(c). Finite element mesh, very refined crack tip region.

3. Loading record and calculation of J

Shear stress (τ) was applied in 104 increments of 1 MPa each. General yield of the ligament occured at an applied shear (τ_{GY}) of 82 MPa, at which load the mean shear (τ_m) across the ligament was 164 MPa. This compares to the shear yield stress of $\tau_0 = \sigma_0/\sqrt{3} = 121$ MPa. The load-displacement curve is shown in Fig. 2. The displacement plotted is the x displacement of the face AB relative to the fixed midside node of face BC. Because the x-displacement varies along the face AB, a weighted mean (conjugate) displacement has been defined for which the work done δU in increasing the conjugate displacement by δD is given by,

$$\delta U = 2F\delta D \tag{7}$$

and F is the total load on face AB.

A second analysis was performed, to the same maximum load of 104 MPa, using an increased crack length of $a = 55$ mm ($a/W = 0.55$). The mesh for this analysis was obtained from that of Fig. 1(a) by translating the refined region along the x-direction by 5 mm, the geometry of the crack tip elements, therefore, being the same for the two analyses. The fracture parameter J is then evaluated using the identification

$$J = -\partial U/\partial A)_D, \quad \text{ie,}$$

$$J = \frac{U(a/w = 0.50) - U(a/W = 0.55)}{5\ \text{mm}^2} \tag{8}$$

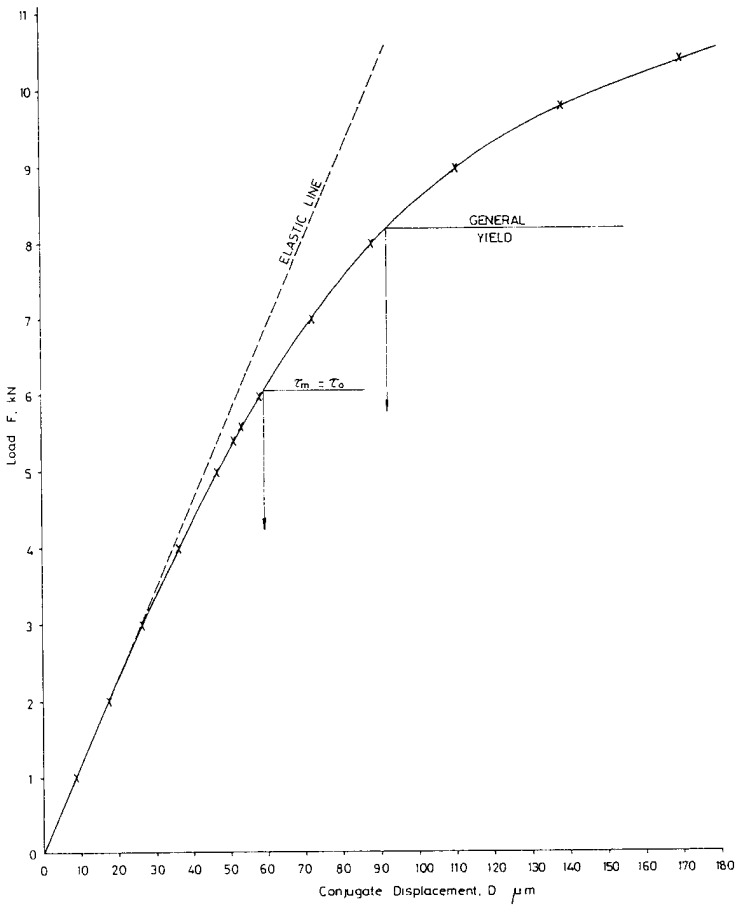

Figure 2. Load-displacement curve.

where U refers to the same conjugate displacement for the two crack lengths, and J applies roughly to the mean crack length ($a = 52.5$ mm). Note that $J = -\partial U/\partial A)_D$ is rigorously true only for deformation theory (non-linear elasticity). However, for monotonic loading using incremental theory our calculation of J should be quite accurate. The results are given in Table 1. To calculate J at $a/w = 0.50$ a small correction has been applied based on the elastic results at $a/w = 0.50$ and 0.55. The fracture parameter K_r is defined as,

$$K_r = \sqrt{\frac{J\,(\text{LEFM})}{J\,(\text{elastic-plastic})}} \tag{9}$$

where the two J's are evaluated at the same applied load (τ). Note that the elastic results give a normalized stress intensity factor, $K/\tau\sqrt{\pi a}$, of 1.38 for $a/w = 0.525$.

Interestingly, J is very accurately proportional to the square of the displacement up to general yield, as shown in Fig. 3. Consequently, J equals J (LEFM) up to general yield as long as these quantities are evaluated at the same displacement. In contrast, at the general yield load ($\tau = \tau_{GY} = 82$ MPa), J (LEFM) is only 60% of J. The close agreement of J with J (LEFM) when evaluated at the same displacement has been noted previously, e.g., by Riccardella and Swedlow [12] for a centre crack tension geometry.

4. Crack tip fields

Figures 4 and 5 plot the shear stress and engineering shear strain along the ligament ($\theta = 0$) against the normalised distance from the crack tip, $R = r\sigma_0/J$. Also shown in these figures are the HRR fields as given by Shih [10] for the same conditions as assumed in our analysis (i.e., mode II, infinitesimal strain theory, $n = 3$ power law hardening and plane strain constraint). Apart from a slight degree of scatter, the FE data at all the loads plotted, from $\tau = 50$ MPa to 104 MPa, lie on the same curve and agree well with the HRR fields. It was also verified that the HRR fields were obeyed for smaller loads, i.e., for plastic zones, extending over less than 30% of the ligament. The latter constitutes a check of the finite element program's ability to correctly evaluate the crack tip fields, since, in small scale yielding, the HRR field is the known solution.

In practice, the process zone is likely to be very much smaller than the $R < 55$ range plotted in Figs. 4 and 5. The process zone will probably be contained within a region of size $R < 5$, and possibly even within $R < 1$, [5,6,7,11]. Consequently the shear stress and

Table 1. Elastic-plastic fracture parameters

τ MPa	$J(0.525)$ N/mm	$J(0.50)$ N/mm	$J(0.50)/\sigma_0$ μm	τ_m/τ_0	τ/τ_{GY} $a/W = 0.525$	Kr
10.1	0.140	0.129	0.614	0.175	0.129	0.995
20	0.561	0.517	2.46	0.347	0.255	0.985
30	1.30	1.20	5.71	0.521	0.382	0.969
40	2.44	2.24	10.69	0.695	0.510	0.945
50	4.08	3.76	17.89	0.868	0.637	0.912
54	4.89	4.50	21.44	0.938	0.688	0.900
56	5.34	4.92	23.42	0.972	0.713	0.894
60	6.15	5.66	27.0	1.042	0.764	0.892
70	9.40	8.66	41.2	1.215	0.892	0.842
80	14.04	12.93	61.6	1.389	1.019	0.787
90	21.01	19.35	92.1	1.563	1.146	0.724
98	28.31	26.07	124.1	1.702	1.248	0.679
104	35.31	32.52	154.8	1.806	1.325	0.645

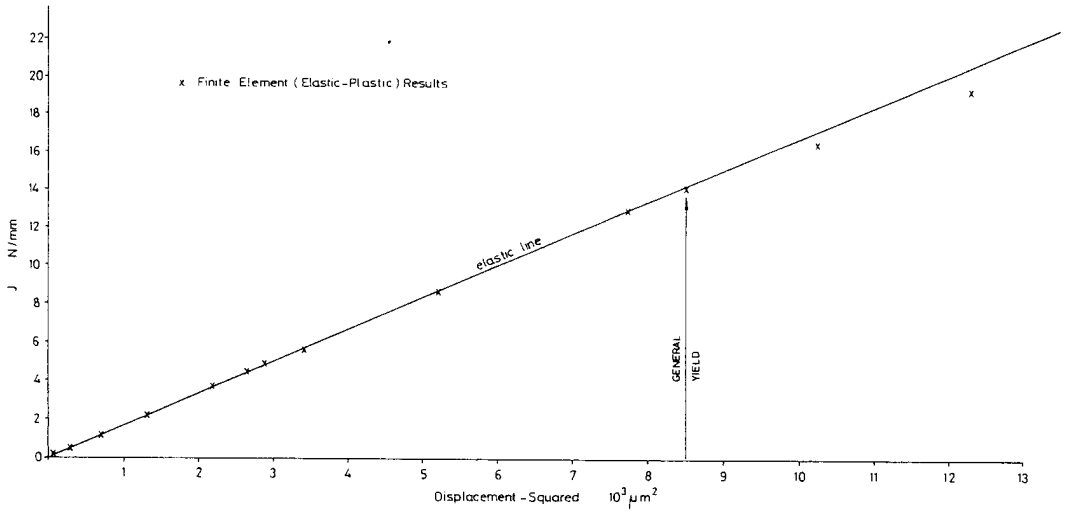

Figure 3. J versus square of displacement up to general yield only.

engineering shear strain on $\theta = 0$ have been plotted in Figs. 6 and 7 within the distance $R < 5$ of the crack tip. The FE data still agree quite well with the HRR fields, although the scatter is greater. It is not suprising that a finite element technique produces greater scatter at closer proximity to the crack tip. The FE strains below about $R = 0.4$ are smaller than the HRR values, but this is almost certainly a result of FE inaccuracy. Figures 8 and 9 plot the θ-components of stress and strain on $\theta = 45°$ against R, together with the HRR fields from [10], within $R < 5$. The FE results are again in good agreement with the HRR fields at all loads, apart from some random scatter.

Some confidence that the scatter in Figs. 4–9 is numerical in origin may be gained by noting that alternate data points (at a given load), which correspond to corner and midside nodes, tend to form separate populations, the one lying at larger stress/strain than the other. As remarked above only a rather small number of elements were used in the mesh and hence adjacent elements near the crack tip have significantly different sizes in order to achieve the very small crack-tip element size. It is therefore to be expected that the use of a larger number of elements, reducing the size-ratio of adjacent elements, would tend to make the corner and midside node results converge, and hence to reduce the scatter.

5. Conclusions

The above results have shown that, for the mode II loading analysed, the crack tip fields are uniquely determined by the single parameter J for loads beyond general yielding ($\tau_{MAX}/\tau_{GY} = 1.27$) and equal to the HRR fields. This demonstrates that an initiation value of J may, in principle, form a valid measure of the toughness of a ductile material in mode II in the same way as for mode I, even when obtained from tests carried beyond general yield. However, there are three provisos to add to this.

(a) Firstly we have studied only one loading geometry, and this idealized loading may be hard to approximate in the laboratory. Furthermore, achievable geometries may give significantly different results. Analysis of practical geometries is therefore desirable, and will hopefully form the basis of future work.

(b) Assuming the above loading to be achievable, the present analysis has been extended only to loads such that $L\sigma_0/J = 320$ (where $L = 50$ mm is the ligament

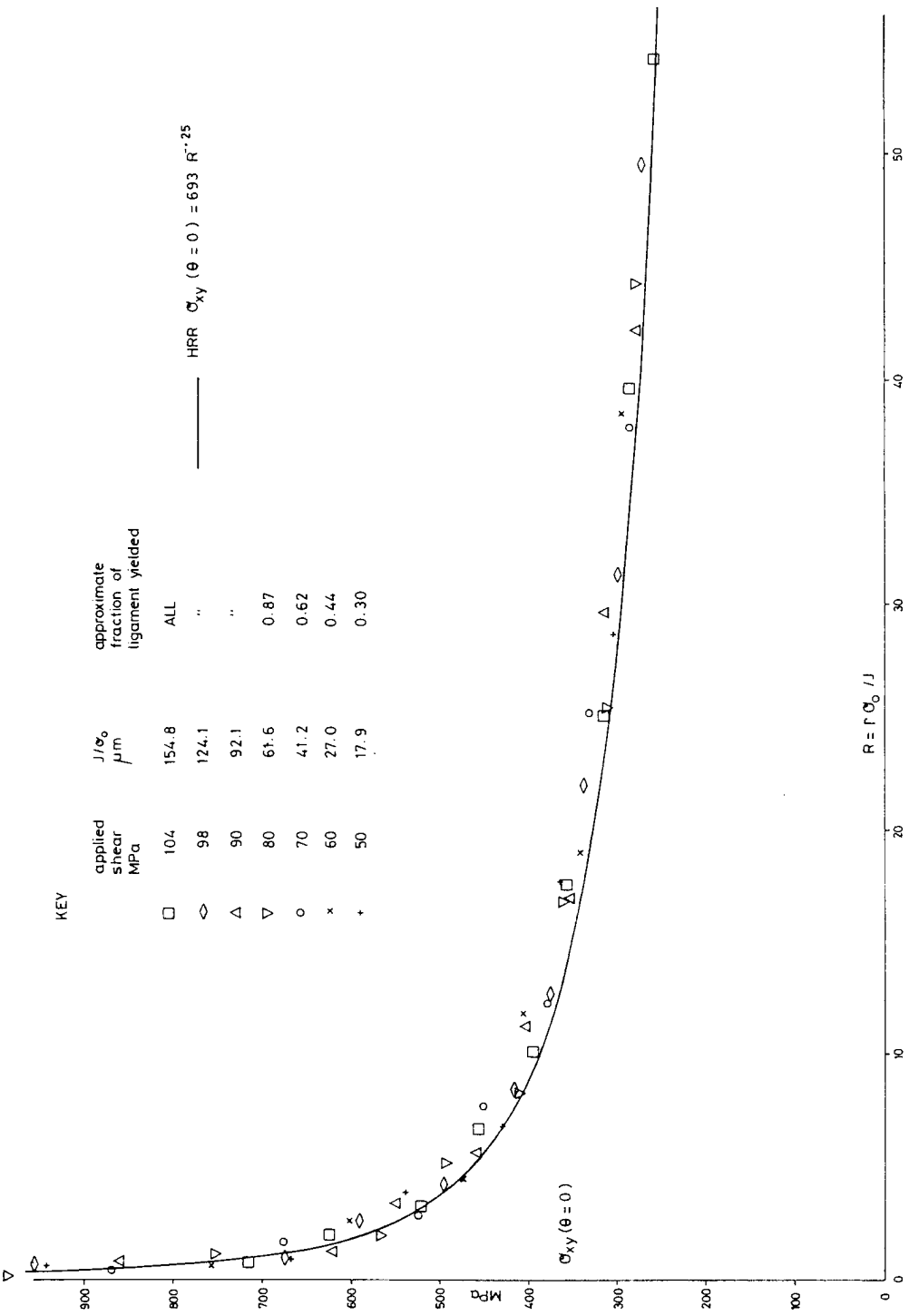

Figure 4. Shear stress on the ligament, $\theta = 0$, versus dimensionless distance from crack tip, R, up to $R = 55$.

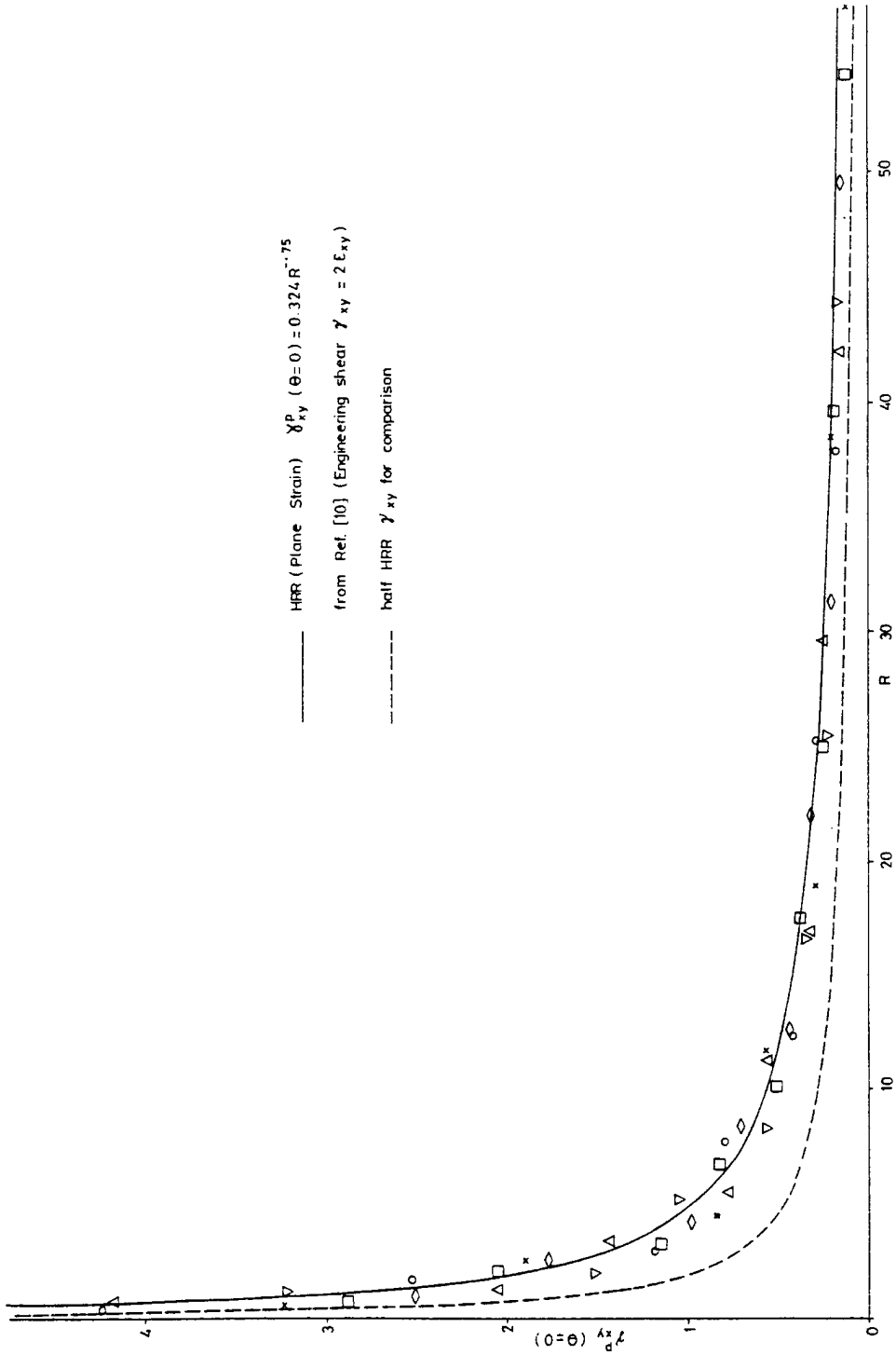

Figure 5. Engineering shear strain on the ligament versus dimensionless distance, R, up to $R = 55$.

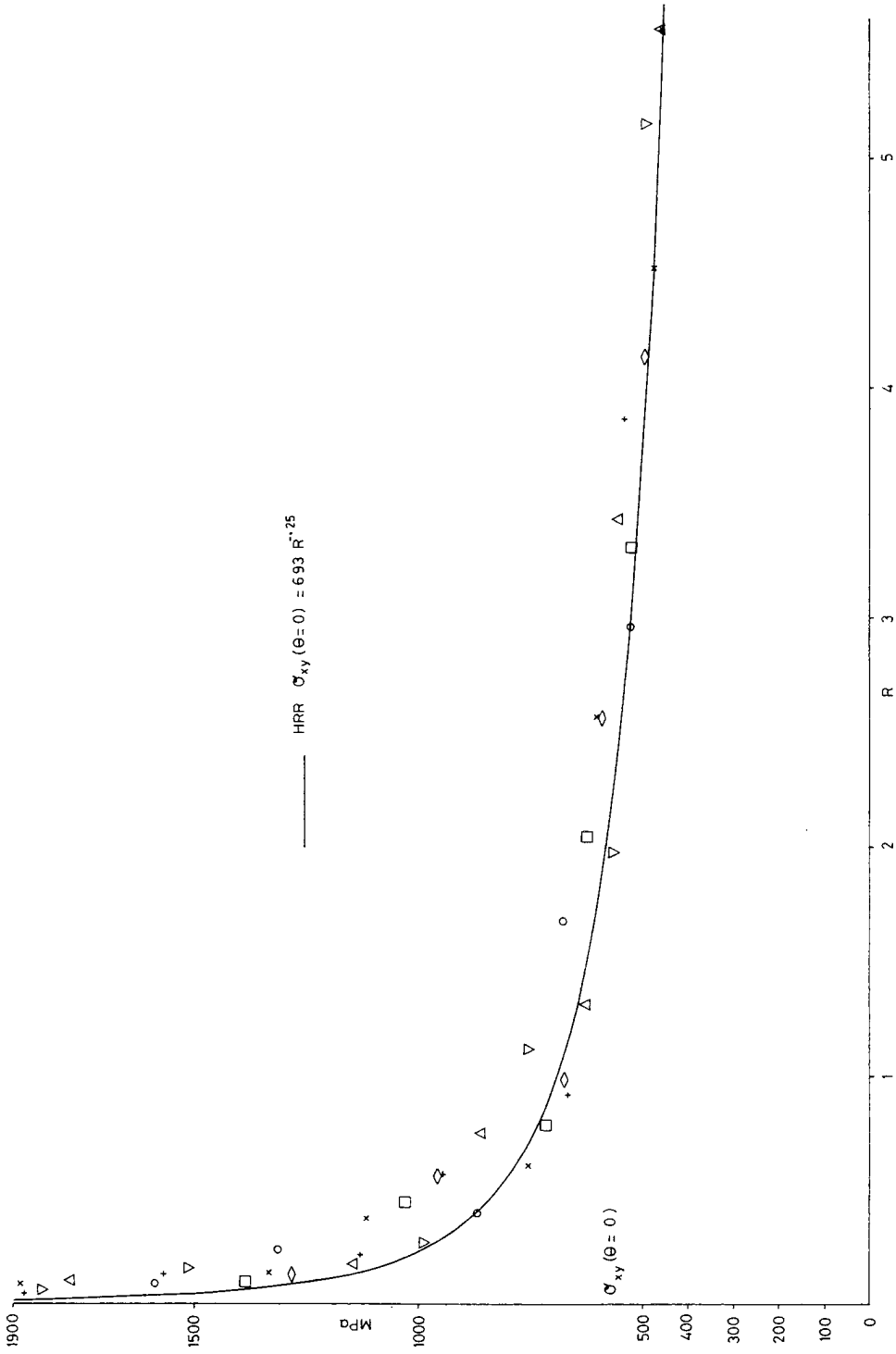

Figure 6. Shear stress on the ligament versus dimensionless distance, R, up to $R = 5.5$.

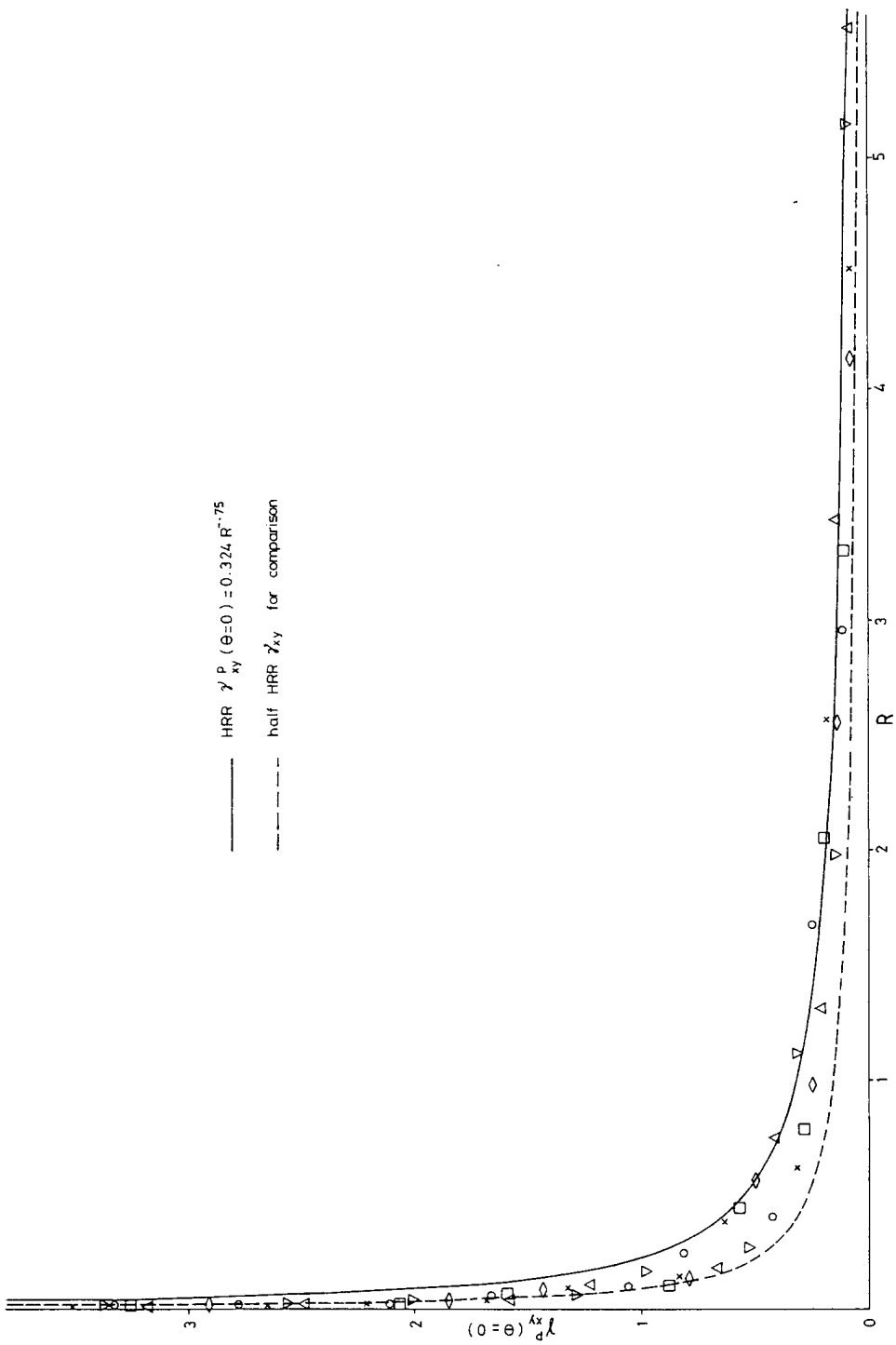

Figure 7. Engineering shear strain on the ligament versus dimensionless distance, R, up to $R = 5.5$.

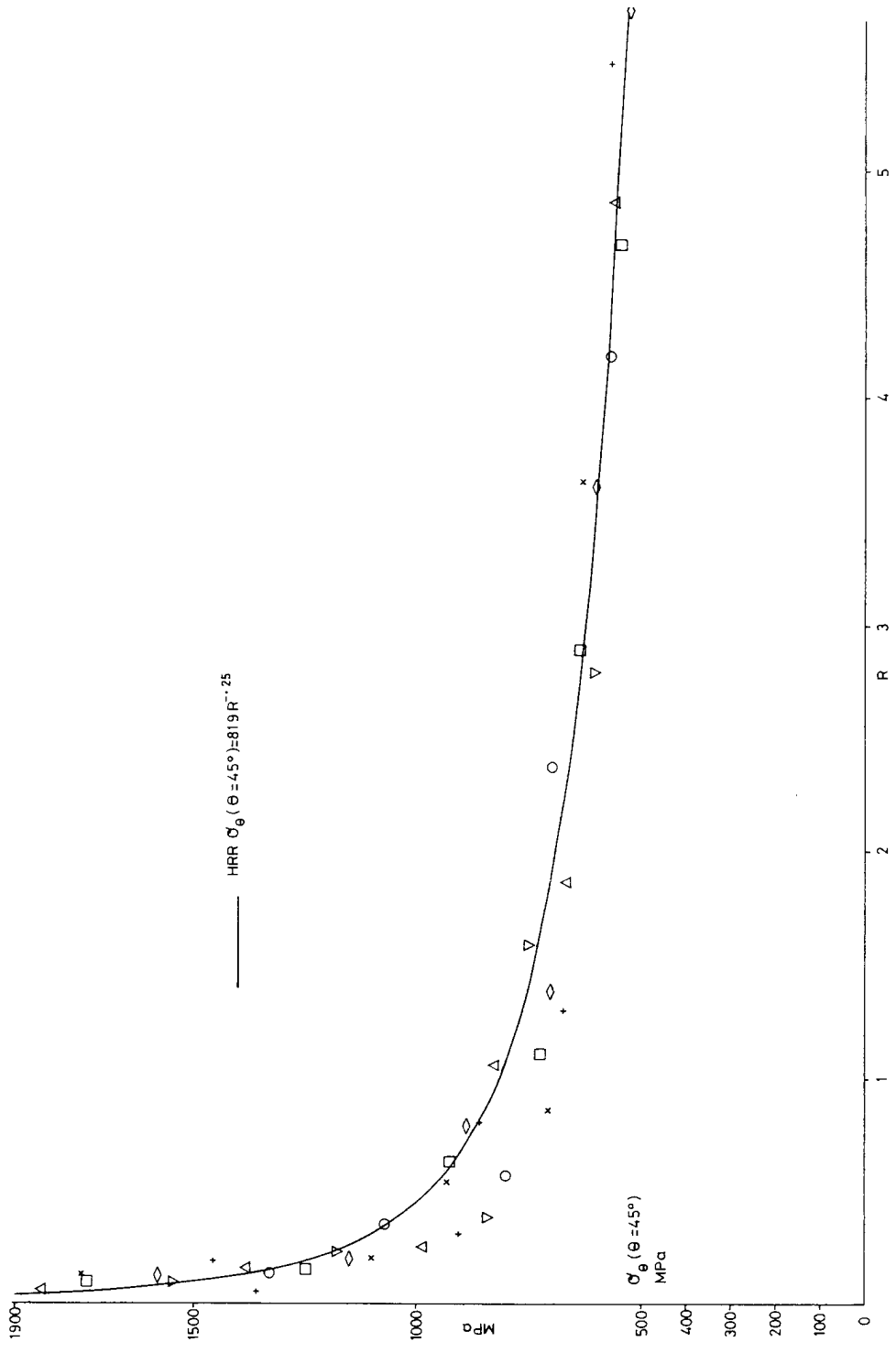

Figure 8. Theta-stress on the line $\theta = 45°$ versus dimensionless distance, R, from the crack tip.

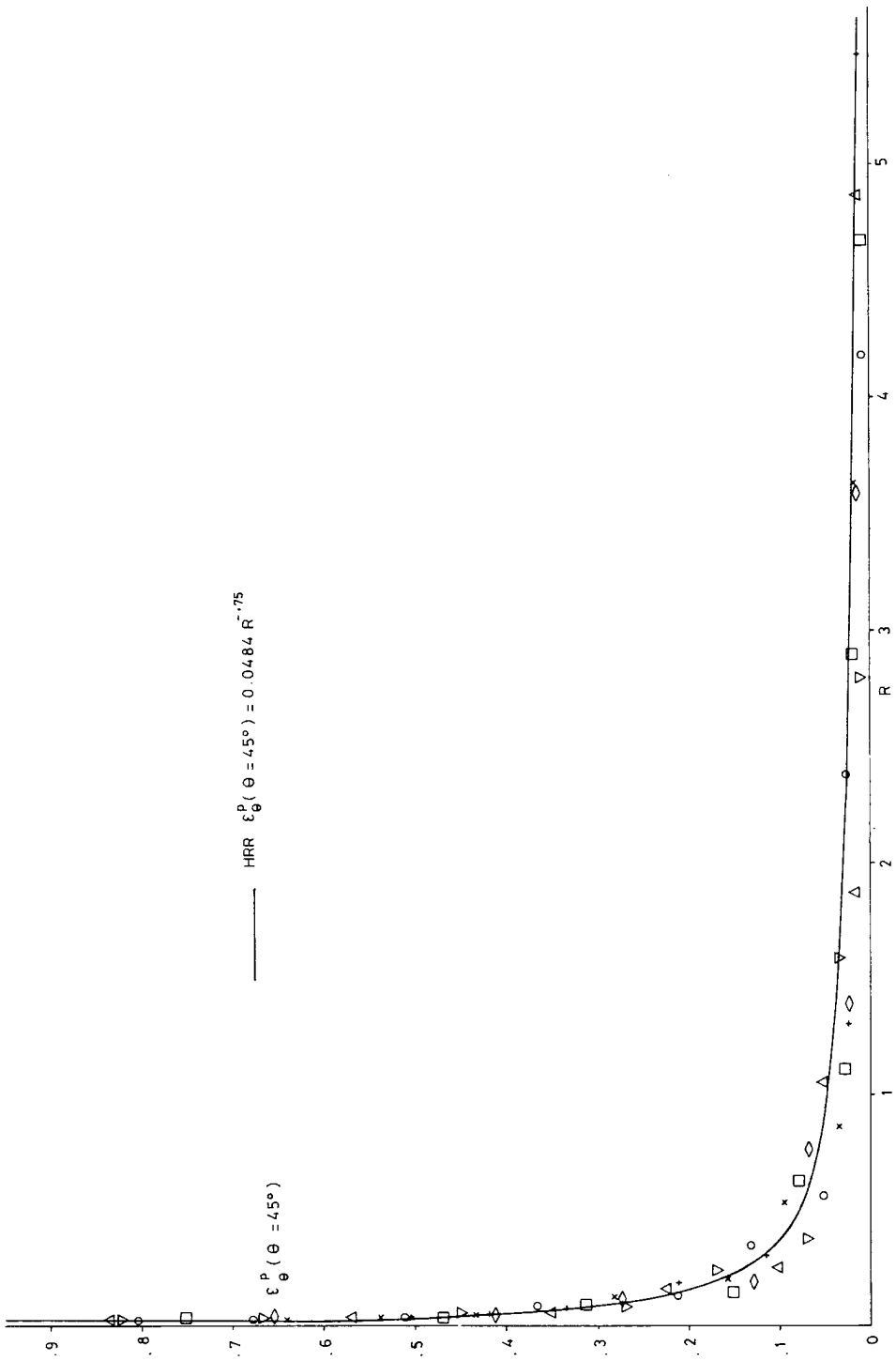

Figure 9. Theta-strain on the line $\theta = 45°$ versus dimensionless distance, R.

size). Thus, for the suggested size of specimen, and for $\sigma_0 = 210$ MPa, validity has been demonstrated only up to toughnesses of 87 MPa $\sqrt{m}$. For tougher materials it would be useful to analyse a larger load. However, in Figs. 4 to 9 there is no sign of the FE results starting to drift away from the HRR fields at the larger loads, and hence it is probable that validity could be demonstrated for $L\sigma_0/J$ substantially less than 320. However, it is sensible to leave this refinement for the analysis of an achievable geometry. The present work has confirmed the possibility, in principle, of valid mode II toughness J-testing in the general yield regime.

(c) Lastly, the present analysis has been confined to an idealized hardening behaviour with $n = 3$. A more stringent test of validity would involve the use of a larger n. Alternatively, a realistic stress-strain relation could be employed, rather than a power law idealization, since this is clearly the case of interest. However, this has the disadvantage that no independent calculation of the small scale yielding field for such material behaviour may be available for purposes of comparison. This also will be the subject of future work.

Acknowledgements

The author is grateful to the Director General of the Central Electricity Generating Board, South Western Region, for permission to publish this paper.

References

[1] J.W. Hutchinson, *Journal of the Mechanics and Physics of Solids* 16 (1968) 13–31, 337–347.
[2] J.R. Rice and G.F. Rosengren, *Journal of the Mechanics and Physics of Solids* 16 (1968) 1–12.
[3] J.D. Eshelby, "The Energy-Momentum Tensor in Continuum Mechanics", in *Inelastic Behaviour of Solids*, ed. M.F. Kanninen et al., McGraw-Hill, New York (1970).
[4] J.R. Rice, *Journal of Applied Mechanics* 35 (1968) 379–386.
[5] R.M. McMeeking and D.M. Parks, in *Elastic-Plastic Fracture*, ASTM STP 668 (1979) 175–194.
[6] C.F. Shih and M.D. German, *International Journal of Fracture* 17 (1981) 27–43.
[7] A. Needleman and V. Tvergaard, *Crack Tip Stress and Deformation Fields in a Solid with a Vertex on its Yield Surface*, US Department of Energy Contract DE-AC02-80-ER10556, Technical Report 87, Brown University (1981).
[8] T.K. Hellen and S.J. Protheroe, in *Computer Aided Design* 6 (1974) 15–24.
[9] T.K. Hellen, in A *Second International Conference on Numerical Methods in Fracture Mechanics*, Swansea, Pineridge Press (1980) 401–415.
[10] C.F. Shih, in *Fracture Analysis*, ASTM STP 560 (1974) 187–210.
[11] C.F. Shih, *Journal of the Mechanics and Physics of Solids* 4 (1981) 305–326.
[12] P.C. Riccardella and J.L. Swedlow, in *Fracture Analysis*, ASTM STP 560 (1974) 134–154.

Résumé

Le programme d'éléments finis BERSAFE est utilisé pour l'analyse d'une plaque carrée fissurée à ses bords et soumise en régime élastoplastique à une sollicitation de mode II. On suppose un état plan de déformation et un écrouissage régi par une loi de puissance $n = 3$. On étudie les champs de contraintes et de déformations à l'extrémité des fissures et on montre que ces champs sont équivalents à ceux décrits par Hutchinson, Rice et Rosengren (HRR) pour toute la gamme de mise en charges allant de la plastification locale de faible envergure à la plastification généralisée.